

# Low-Dimensional Nanostructure Ultraviolet Photodetectors

Lin Peng, Linfeng Hu, and Xiaosheng Fang\*

Low-dimensional (LD) nanostructures are ideal systems for constructing high-performance photodetectors due to their tailored geometries, high surface-area-to-volume ratios and rationally designed surfaces. This article provides a brief summary about recent progress on LD nanostructures based visible-light-blind ultraviolet photodetectors. The current challenges and an outlook on the future developments of this research field are summarized and highlighted.

## 1. Introduction

Ultraviolet (UV) light is part of the electromagnetic radiation spectrum; its spectral range starts from the visible (400 nm; ca. 3.1 eV) and reaches the X-ray spectral low energy frontier (10 nm; ca. 124 eV). The UV radiation emitted from the sun can be divided into four spectral regions. The longest wavelength—the UV-A band (ca. 320–400 nm)—can reach the earth's surface. The UV-B band (ca. 280–320 nm) light is absorbed by the molecules in sunscreens, so that human skin can be decently protected. The UV-C band (ca. 200–280 nm) light is completely absorbed by the earth's atmosphere and does not reach the ground. The far UV spectrum—located in the range 10–200 nm—needs a high level of vacuum to propagate, and for that reason is very commonly called “vacuum UV” (VUV). 98.7% of the UV radiation that reaches the earth's surface is UV-A.<sup>[1]</sup> Much research has shown that UV-A light may cause skin cancer. Therefore, the development of novel effective UV photodetectors (PDs) that exhibit high UV-A band sensitivity but are blind towards standard visible radiation is of great importance. Meantime, visible-blind deep-ultraviolet (DUV) PDs have vast potential applications in the fields of solar astronomy, missile plume detection, space-to-space transmission, fire alarms, and combustion monitoring,<sup>[2–4]</sup> since their operating spectral range (220–280 nm) avoids interference from solar radiation.<sup>[2]</sup> The ideal PD for such applications is generally designed to display a high responsivity, a good linearity of the photocurrent as a function of the incident optical power, a low noise level, and good visible rejection (i.e., high spectral selectivity). A short response time can also be of great importance in applications where a real-time fast signal treatment is necessary. Narrow bandgap semiconductors, such as silicon and some III–V compounds (GaP, GaAsP) having

bandgaps typically located in the infrared (Si) or in the visible red (GaAsP), were first considered to perform UV detection; however, the insertion of costly high-pass optical filters and phosphors is necessary in such applications in order to tune the photodetecting system to the appropriate spectral range and prevent degradation of devices on exposure to UV light with energies much higher than the semiconductor bandgap. Moreover, for high-

sensitivity application, these devices need to be cooled to reduce the dark current.

Recently, the use of low-dimensional (LD) wide-bandgap inorganic semiconductor nanostructures materials with tailored geometry as building blocks for visible-blind UV PDs has attracted intense attention. The electrical integration of synthesized LD nanostructures has been achieved with lithography and optical integration, which promises high speeds and greater device versatility.<sup>[5]</sup> LD nanostructures can be divided into zero-dimensional (0D, when they are uniform), 1D (when they are elongated), and 2D (when they are planar), based on their shapes and morphologies.<sup>[1]</sup> These wide-bandgap semiconductor nanostructures, such as quantum dots, nanotubes, nanowires, nanorods, nanobelts/nanoribbons, nanocables, core/shell structures, nanostructure arrays, epitaxial film, heterostructures, and so forth, are expected to play key roles in visible-blind UV PDs. Compared with UV PDs based on traditional thin-film and bulk materials, UV PDs based on LD semiconductor nanostructures usually have an advantage of higher responsivity and photoconductive gain because of their high surface-area-to-volume ratios (SVRs) and the reduced dimension of the effective conductive channel.<sup>[6–8]</sup> Generally, a large SVR can significantly increase the number of surface trap states and prolong the photocarrier lifetime, and the reduced dimensionality can confine the active area of the charge carrier and shorten the transit time.<sup>[9]</sup> For fabrication of visible-blind UV PDs, many wide-bandgap materials—including nitride compounds (e.g., GaN) and metal oxides (e.g., ZnO-based materials)—having bandgap values are larger than about 3.30 eV are suitable for the building blocks of visible-blind UV PDs;<sup>[10–29]</sup> furthermore, various device structures—such as photoconductive, Schottky barrier, p–n (or p–i–n), and metal–semiconductor–metal (MSM)—have been adopted for preparing UV PDs.<sup>[30–44]</sup> In particular, for the PDs having MSM structures, two kinds of devices have been demonstrated: Schottky-contact-based photovoltaic or ohmic-contact-based photoconductive devices; compared to photovoltaic detectors, it is usually easier to achieve higher gain with photoconductive ones, while they show slow response times because of possible persistent photoconductivity effects.<sup>[45]</sup>

Dr. L. Peng, Dr. L. F. Hu, Prof. X. S. Fang  
Department of Materials Science  
Fudan University  
Shanghai 200433, PR China  
E-mail: xshfang@fudan.edu.cn



DOI: 10.1002/adma.201301802

This article provides a brief summary of the state-of-the-art research activities that focus on wide-bandgap semiconductor nanostructure-based visible-blind UV PDs. We begin by introducing the methods for the fabrication of UV PD devices, then discuss the recent efforts and great development in the performance and applications of LD nanostructure-based UV PD devices, and finally propose the possible challenges and opportunities that researchers in this field are facing.

## 2. Low-Dimensional Nanostructure UV PDs

In general, UV PDs are fabricated by two processes: the synthesis of semiconductor nanostructures and the construction of nanostructure-based devices. During the past decade, many methodologies have been developed to synthesize inorganic semiconductor nanostructures.<sup>[46–49]</sup> They are commonly placed into two categories, namely, the bottom-up approach in which the functional structures are assembled from individual atoms and molecules, and the top-down approach that relies on dimensional reduction by a combination of lithography, etching, and deposition to form functional devices and their integrated systems.<sup>[50]</sup> Although both approaches have been exceedingly successful for making inorganic semiconductor nanostructures with different advantages and disadvantages, currently most inorganic semiconductor nanostructure-based nanodevices are fabricated via the facile combination of both strategies. Up to now, template-assisted growth, epitaxial growth, homoepitaxial growth, heteroepitaxial growth, conversion from other nanostructures, thermal evaporation, evaporation–condensation, plasma-assisted metal–organic chemical vapor deposition (MOCVD), vapor–liquid–solid (VLS) and vapor–solid (VS) processes, and hydrothermal/solvothermal reaction and subsequent heat-treatment processes have been successfully developed to synthesize semiconductor nanostructures. When semiconductor nanostructures are synthesized, the electrodes are subsequently deposited on the as-fabricated nanostructures on a prepared substrate by using optical lithography with the assistance of a pre-designed mask and electron beam deposition.

### 2.1. 2D Nanostructures

Developments in epitaxial film growth technology have led to the realization of visible-blind PDs operating in the UV spectral region. Because of a concern of skin cancer, a type of effective visible-blind UV-A PDs are emerging. Typically, ZnO, an environmentally friendly semiconductor with a room-temperature band gap of 3.37 eV, is an excellent candidate for UV detection because of its various synthetic methods, diverse processing technologies, radiation hardness, high temperature resistance, low growth cost, and vast potential for modulation of its bandgap through doping techniques.<sup>[42–44]</sup> By growing high-quality ZnO epitaxial films on sapphire substrates, fabricated Schottky UV-A PDs exhibit fast response speed (microsecond scale).<sup>[51]</sup> On the other hand, solar-blind DUV PDs based on wide-bandgap semiconductor films, such as AlGaN, ZnMgO, diamond, LaAlO<sub>3</sub>, MgZnS, and  $\beta$ -Ga<sub>2</sub>O<sub>3</sub> have been investigated

and show the possibility of developing DUV PDs with intrinsic 'visible-blindness' and enabling room-temperature operation.<sup>[40–44,52–54]</sup> For visible-blind DUV PDs, the cutoff working wavelength should be lower than 280 nm, corresponding to a bandgap wider than 4.4 eV. Currently, diamond (ca. 5.5 eV) DUV PDs are commercially available.<sup>[55]</sup> Diamond film-based UV PDs most commonly refer to microwave plasma assisted-CVD-grown polycrystalline diamond photoconductors, which exhibit a discrimination ratio up to 10<sup>8</sup> between 210 nm and visible light, and a short time response typically lying in the nanosecond range.<sup>[40]</sup> In recent years, the bandgap modulation of ZnO films by alloying with a wider bandgap semiconductor MgO (7.8 eV) has been widely investigated.<sup>[42–44]</sup> A Schottky-type MSM visible-blind UV PD fabricated on high-quality wurtzite Mg<sub>0.55</sub>Zn<sub>0.45</sub>O epitaxial film,<sup>[44]</sup> showed a responsivity peak of 22 mA W<sup>-1</sup> under 130 V bias. A sharp cutoff was recognized at a wavelength of 270 nm, and a temporal response measurement indicates a fast decay time of less than 500 ns.

However, although some significant improvements have been recently achieved in the field, the development of this special range of PDs has been somehow hindered. Achieving high crystal quality of superconductor thin film is still challenging because of the lack of high-quality and low-cost substrates for lattice-matched growth. Most semiconductor epitaxial films deposited by metal–organic chemical vapor (MOCVD) deposition, pulsed laser deposition (PLD), or radio-frequency sputtering (RFS) have a large density of dislocations and grain boundaries. Transport and UV photoconduction in these polycrystalline semiconductor films depends sensitively on stoichiometry and trap densities. A slow response time of many UV PDs based on polycrystalline semiconductor epitaxial films, ranging from a few minutes to several hours, is commonly observed.<sup>[56,57]</sup> Therefore, the development of epitaxial film-based UV PDs needs a further breakthrough addressing these technical difficulties.

### 2.2. 1D Nanostructures

1D semiconductor nanostructures, such as nanowires, nanorods, and nanobelts, are attractive building blocks for a new generation of high sensitivity and selectivity UV PDs primarily because of their high SVRs and diverse functions as both device elements and interconnects. Some important wide-bandgap semiconductors, including ZnO, ZnS, Nb<sub>2</sub>O<sub>5</sub>, SnO<sub>2</sub>, etc, are potential candidate materials for applications in 1D nanostructure-based UV-A PDs.<sup>[7,11,30,32,35]</sup> We tabulate representative results on the properties of 1D nanostructure-based UV PDs reported so far, along with a brief description of the corresponding device continuations, detection wavelengths, and PD performance (Table 1). As summarized in Table 1, tremendous progress has already been made in the fabrication of 1D nanostructure-based UV PDs. In particular, ZnO nanowires produced by CVD technology have been investigated by several groups for UV PD applications.<sup>[11–18]</sup> Their results show that, for a range of different synthesis conditions and device processing, the conductivities of ZnO nanowires are sensitive to UV light exposure. Despite the widespread research into 1D ZnO nanostructure-based UV PDs, their performances are

Table 1. LD nanostructure-based UV PDs.

Photodetector	UV light	Bias	Dark current	Photocurrent	Rise time	Decay time	Ref.
ZnO nanowire	390 nm	5 V	1–10 nA	100 $\mu$ A	—	—	[11]
ZnO nanowire	365 nm	0–5 V	ca. 1 pA	ca. 250 nA	<1 s	<1 s	[12]
ZnO nanowire	325 nm	5 V	ca. 15 pA	0.28 nA	43.7 s	—	[13]
ZnO microtube	365 nm	5 V	1.5 $\mu$ A	0.135 mA (air)	5.9 s	638 s	[14]
ZnO nanowire	365 nm	1 V	0.04 nA	60 nA	0.6 s	6 s	[15]
ZnO nanowire array	370 nm	5 V	70 $\mu$ A	100 $\mu$ A	0.4 ms	—	[16]
ZnO nanorod	325 nm	2 V	1 nA	22 nA	3.7 s	63.6 s	[17]
ZnO nanorod	254 nm	0.2 V	ca. 2 nA	2.4 $\mu$ A	—	30 min	[18]
ZnO nanowire	365 nm	2 V	2 $\mu$ A	15 $\mu$ A	45 s	55 s	[19]
ZnS nanobelt	320 nm	5 V	<1 pA	1 pA	<0.3 s	<0.3 s	[7]
ZnS nanobelt array	320 nm	5 V	ca. 3 pA	ca. 2 nA	2.57 ms	1.99 ms	[35]
SnO <sub>2</sub> nanobelt	254 nm	–5 V	0.4 nA	80 $\mu$ A (air)	—	—	[20]
SnO <sub>2</sub> nanowire	325 nm	0.1 V	30 nA	210 nA (air)	—	—	[21]
SnO <sub>2</sub> nanowire array	365 nm	12 V	77 $\mu$ A	130 $\mu$ A	—	—	[22]
SnO <sub>2</sub> nanowire	320 nm	1 V	19.4 nA	2.1 $\mu$ A	—	—	[32]
ZnO-functional SnO <sub>2</sub> nanowire	365 nm	5 V	200 nA	300 nA	—	—	[23]
Nb <sub>2</sub> O <sub>5</sub> nanobelt	320 nm	1 V	ca. 10.6 pA	ca. 100 pA	—	—	[30]
In <sub>2</sub> Ge <sub>2</sub> O <sub>7</sub> nanobelt	230 nm	5 V	—	ca. 19 nA	<3 ms	<3 ms	[36]
$\beta$ -Ga <sub>2</sub> O <sub>3</sub> nanowire	254 nm	8 V	15 pA	10 nA	0.22 s	0.09 s	[24]
In <sub>2</sub> O <sub>3</sub> nanowire	254 nm	0.3 V	—	290 nA	10 s	—	[25]
CeO <sub>2</sub> nanowire film	254 nm	5 V	0.25 pA	0.44 nA (H <sub>2</sub> O)	2 s	—	[26]
ZnSnO <sub>3</sub> nanowire	UV	3 V	0.3 nA	162 nA	20 s	—	[27]
ZnGa <sub>2</sub> O <sub>4</sub> nanowire	254 nm	30 V	8.5 pA	1 nA	—	—	[28]
Colloidal ZnO nanoparticles	370 nm	120 V	0.2 nA	5.5 $\mu$ A	1.3 s	2 min	[37]
ZnO nanoparticles film	350 nm	5.0 V	50 nA	2.6 $\mu$ A	467 $\mu$ s	940 $\mu$ s	[34]
SnO <sub>2</sub> -coated ZnO nanowire	325 nm	0.8 V	ca. 31 nA	ca. 140 nA	1.5 s	ca. 25.6 s	[29]
ZnS/ZnO nanobelt (Device I)	320 nm	5.0 V	0.67 $\mu$ A	4.64 $\mu$ A	<0.3 s	1.7 s	[31]
ZnS/ZnO nanobelt (Device II)	320 nm	5.0 V	3.03 $\mu$ A	17.76 $\mu$ A	<0.3 s	1.5 s	[31]
ZnS/ZnO nanofilm (Device I)	370 nm	5.0 V	15.1 nA	18.0 $\mu$ A	—	—	[33]
ZnO/ZnS nanofilm (Device II)	370 nm	5.0 V	15.1 nA	2.94 $\mu$ A	—	—	[33]
ZnO quantum dot/graphene	365 nm	3.0 V	ca. 0.72 mA	ca. 10 mA	50 s	1 s	[38]
P <sub>3</sub> HT:ZnO nanocomposite	360 nm	–9.0 V	6.8 nA	ca. 70 mA	25 $\mu$ s	558 $\mu$ s	[39]
Self-powered UV PD (I)	UV	0 V	<1 pA	ca. 1 $\mu$ A	30 ms	50 ms	[59]
Self-powered UV PD (II)	325 nm	0 V	<1 pA	ca. 2 $\mu$ A	ca. 20 $\mu$ s	ca. 219 $\mu$ s	[61]

strongly limited by inherent defects, such as oxygen vacancies and zinc interstitials, and absorption–desorption processes at the surface. For practical application, their current intensities and stabilities are far from satisfactory and need to be improved.

ZnS, an alternative semiconductor with wide bandgaps of 3.72 and 3.77 eV for cubic zinc blend (ZB) and hexagonal wurtzite (WZ) forms, respectively, has a higher potential as a UV detector in this UV-A band.<sup>[7,35]</sup> The individual ZnS nanobelt-based UV PD is extremely sensitive to UV light exposure and exhibits a high on-off ratio (Figure 1a), but the photocurrent is unstable and the intensity needs to be improved (Figure 1b).<sup>[7]</sup> A pre-designed patterned substrate was used to fabricate

a horizontal ZnS-nanobelt array-based UV PD made of multiple ZnS nanobelts (Figure 1c).<sup>[7]</sup> In contrast, the corresponding photocurrent intensity of the modified UV PD upon 320 nm light illumination is enhanced about 20 times and the photocurrent stability is also improved significantly (Figure 1d). Furthermore, an alternative approach is the direct integration of 1D ZnS nanobelts into a thin-film-like UV PD (Figure 1e), which possess ultrafast response speed, low dark current, high ratios of photocurrent immediate decay and photocurrent/dark current, and good stability (Figure 1f).<sup>[35]</sup> Additionally, some types of semiconductor material, such as In<sub>2</sub>GeO<sub>7</sub>,  $\beta$ -Ga<sub>2</sub>O<sub>3</sub>, and ZnGa<sub>2</sub>O<sub>4</sub>,<sup>[24,28,36]</sup> have also been used to fabricate 1D nanostructure-based DUV PDs due to great technological interest in the

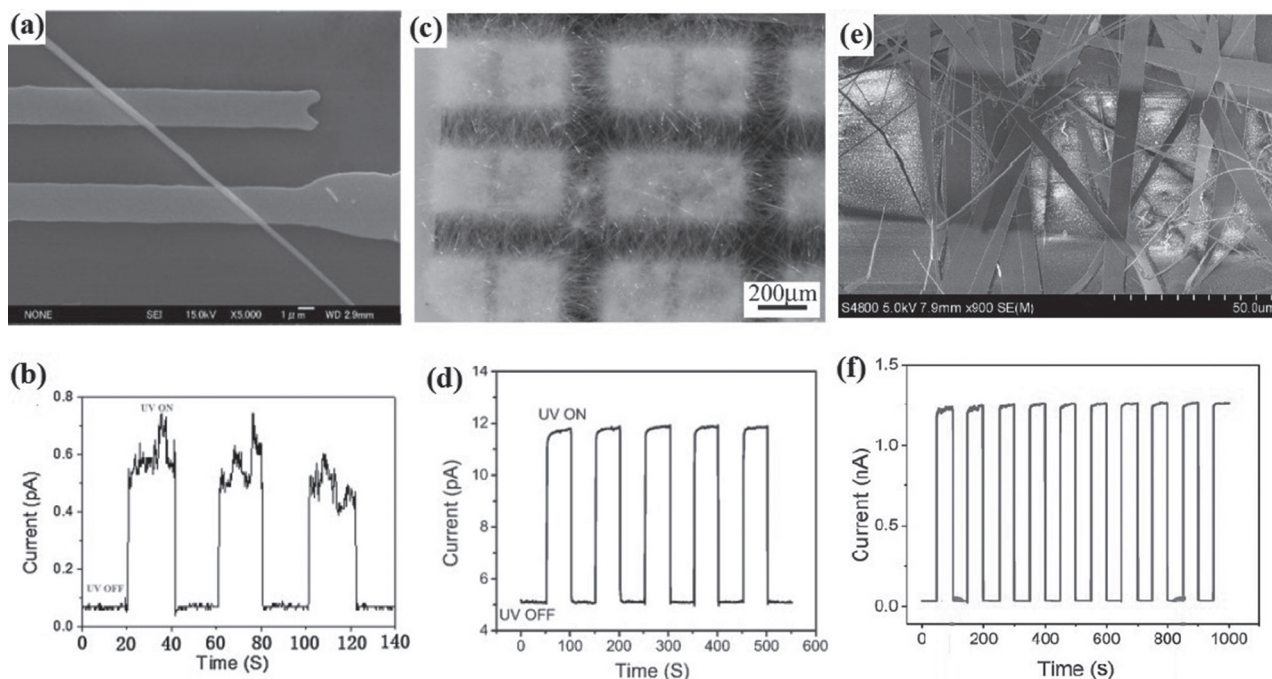


**Figure 1.** ZnS nanostructures-based visible-blind UV-light PDs and the corresponding time responses of the PDs under 320 nm light illumination measured by a current meter under and without UV light: a and b) individual ZnS nanobelt-based sensors; c and d) multiple ZnS-nanobelts; and, e and f) microscale ZnS nanobelt-based sensors (horizontal nanobelt array-based sensors).<sup>[7,35]</sup>

development of luminescence, vacuum electronics, and multicolor emitting phosphors. Among these, high-quality single-crystalline  $\text{In}_2\text{GeO}_7$  nanobelts synthesized by a vapor transport process were recently designed for DUV visible-blind PDs.<sup>[36]</sup> The detectors showed good photoconductive performance under 230 nm light irradiation, namely, high sensitivity and selectivity towards the solar-blind spectrum, excellent stability and reproducibility, fast response and decay times ( $< 3$  ms), high responsivity ( $3.9 \times 10^5 \text{ A W}^{-1}$ ), and good quantum efficiency ( $2.0 \times 10^8\%$ ). Though 1D semiconductor nanostructures have been widely studied to enhance the quantum efficiency and shorten the response time of PDs, the main drawback of fabricating 1D semiconductor nanostructures-based UV PDs is to use time-consuming nanowire manipulation methods and one-by-one fabrication techniques, which make currently them unattractive for large-scale production.

### 2.3. Zero-Dimensional Nanostructures

0D nanostructure-based UV PDs mainly highlight the fabrication of nanofilms based on semiconductor quantum dots or nanoparticles, and the construction of nanofilm-based devices. Technologically, if the quantum dots or nanoparticles could be assembled as a nanofilm form, the metal electrodes can be easily deposited on the nanofilm using a hand-operable metal microwire as a mask, and also the performance of nanofilm PDs utilizing the quantum-size effect will be optimized due to the integration of a large number of nanoparticles.

The use of solution-processed nanofilms of colloidal inorganic semiconductor quantum dots (or nanoparticles) as PDs has been an efficient approach in the quest to fabricate low-cost PDs. The development of synthesis strategies for colloidal ZnO nanocrystals paves the way toward solution-processed ZnO nanocrystalline devices. By spin-coating colloidal ZnO nanoparticles on glass substrates, followed by annealing in air and evaporation of gold contacts, through a shadow mask, a ZnO nanoparticle film-based UV PD was fabricated (Figure 2a).<sup>[37]</sup> The UV PD shows a high photocurrent (ca. 0.2 mA; Figure 2b), and the photoconductive gain is much larger than unity. It is generally accepted that the absorption/desorption of oxygen molecules governs the generation of free carriers for ZnO: i) the oxygen molecules adsorbed onto the hollow-sphere surfaces capture free electrons from the *n*-type ZnO [ $\text{O}_{2(\text{g})} + \text{e}^- \rightarrow \text{O}_{2(\text{ad})}^-$ ], creating a depletion layer near the surface. This reduces the electrical conductivity; and, ii) under UV illumination, electron-hole pairs are generated—the holes migrate to the surface along the potential gradient and combine with oxygen, inducing desorption of oxygen from the ZnO surface [ $\text{h}^+ + \text{O}_{2(\text{ad})}^- \rightarrow \text{O}_{2(\text{g})}$ ] (Figure 2c). The hole-trapping process results in an increase in the free-carrier concentration which in turn reduces the Schottky barrier between contacts and ZnO nanoparticles for electron injection.

The liquid-liquid interfacial self-assembly has been shown to be another efficient and low-cost method to fabricate nanofilm-based PDs; a hollow ZnO sphere nanofilm-based PD has been made using this method.<sup>[34]</sup> The PS-ZnO core-shell nanospheres were dispersed at a hexane-water interface to

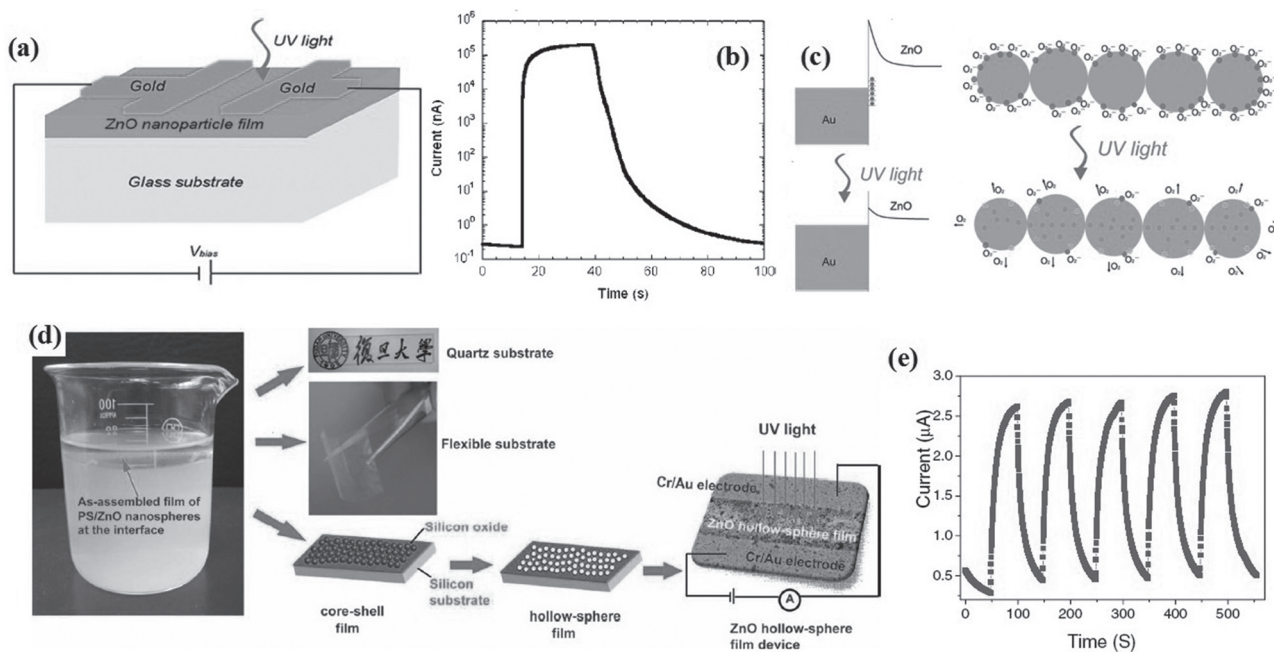


**Figure 2.** a) Schematic of a ZnO nanoparticle film device structure. b) Time-resolved photocurrent at 120 V in response to a 25.5 s light pulse. c) Carrier transport processes in the ZnO nanoparticle film devices. Reproduced with permission.<sup>[37]</sup> Copyright 2008, ACS. d) Schematic illustration of the fabrication procedures for ZnO hollow-sphere nanofilm photodetector: deposition of the as-assembled PS/ZnO precursor film on a silicon substrate with a 200 nm SiO<sub>2</sub> top layer, thermal transformation from a PS/ZnO precursor nanofilm into a ZnO hollow-sphere nanofilm, and a complete ZnO hollow-sphere nanofilm photodetector. e) Response time of the photodetector measured in air at a bias of 5.0 V. Reproduced with permission.<sup>[34]</sup>

form a densely-packed film. The film was transferred onto a SiO<sub>2</sub> (200 nm)/Si substrate, and annealed in air to obtain a ZnO hollow-sphere nanofilm (Figure 2d). A UV PD was then fabricated from the as-transformed ZnO hollow-sphere nanofilm, which shows a high photocurrent (ca. 2.6  $\mu\text{A}$ ) and a fast response (with both rise and decay times of less than 5 s) under 350 nm light illumination (1.32 mW cm<sup>-2</sup>) at an applied voltage of 5.0 V (Figure 2e). The high-performance ZnO nanofilm PD fabricated by this method is very promising for practical application on high-frequency photoelectronic switches and light-sensors due to its excellent sensitivity, stability, and very fast response speed. More importantly, the method can be easily extended to other semiconductor nanospheres, such as ZnS and SnO<sub>2</sub> hollow spheres; new PDs can be expected that are fabricated by this strategy.

#### 2.4. Hetero, Biaxial, and Compound Nanostructures

Semiconducting nanocomposites consisting of several different functional materials are of prime importance for improving device performance. The fabrication of UV photodetectors based on heterostructures or nanocomposite structures will be very valuable due to their multifunctional and property-tuning potential. Recently, a UV-A PD based on a ZnS/ZnO biaxial nanobelt showed a high photocurrent (ca. 4.64  $\mu\text{A}$ ) and a fast response (with response and recovery times of less than 0.3 s and ca. 1.7 s, respectively) under 320 nm light illumination (0.91 mW cm<sup>-2</sup>) at an applied voltage of 5.0 V (Figure 3a and b).<sup>[31]</sup> As summarized

in Table 1, the performance of the present ZnS/ZnO biaxial nanobelt-based UV PD is significantly enhanced compared with that of pure ZnS or ZnO nanostructure-based UV PDs, combining high sensitivity and fast response speed, and justifying the effective utilization of the present ZnS/ZnO biaxial nanobelt as the building blocks of UV PDs. More interestingly, a ZnS/ZnO nanofilm-based UV PD,<sup>[33]</sup> among which well-organized bilayer nanofilms consisting of close-packed semiconducting ZnS and ZnO hollow microspheres were fabricated using an oil-water interfacial self-assembly strategy, displays a very low dark current of 15.1 nA at an applied voltage of 5.0 V, and a photocurrent of 18.0  $\mu\text{A}$  when the wavelength of light source is 370 nm (1.70 mW cm<sup>-2</sup>). Note that the photocurrent of 18.0  $\mu\text{A}$  for the present device is about seven times higher than that for the device constructed from a monolayer film consisting of ZnO microspheres,<sup>[34]</sup> and also superior compared to other PDs including those based on ZnS and ZnO nanostructures (see Table 1). The remarkable enhancement in photocurrent should be attributed to the fact that the bilayer nanofilm-based PDs integrate electrical signals from a large number of ZnS and ZnO hollow microspheres rather than from individual building blocks. Furthermore, the bilayer nanofilms made of ZnS and ZnO hollow microspheres can be regarded as a hetero-structured assembly. The presence of an internal electric field due to the band bending at the heterostructure interface facilitates the separation of electron-hole pairs under UV light illumination, which significantly reduces the electron-hole recombination ratio, resulting in a much higher photocurrent compared with that of the monolayer-film device.

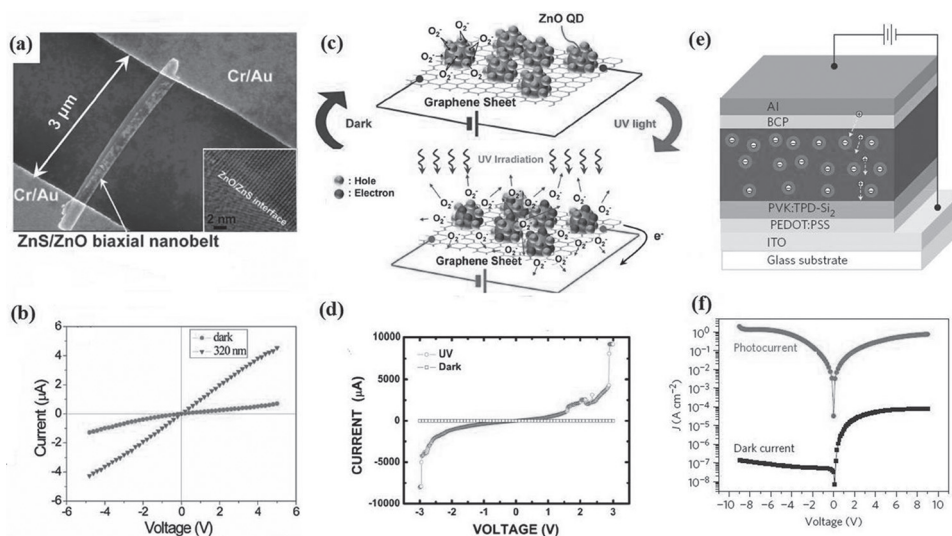


**Figure 3.** a) A representative SEM image of the PD based on ZnS/ZnO biaxial nanobelt with Cr/Au electrodes deposition at the two ends. b)  $I$ - $V$  curves under dark condition and UV-light illumination. Reproduced with permission.<sup>[31]</sup> c) Schematic diagram of the photoresponse mechanisms of the photodetector. d) Currents as functions of the applied voltage ( $I$ - $V$ ) for the UV PD in the dark (rectangles) and under illumination by a 365 nm UV light at a power of 6 W (circles). Reproduced with permission.<sup>[38]</sup> Copyright 2013, AIP. e) Schematic layout of the PVK:ZnO nanocomposite film-based PD structure. f) Photocurrent and dark current density of the PVK:ZnO device. Reproduced with permission.<sup>[39]</sup> Copyright 2012, MPL.

In ultrafast PDs, graphene layers play very important roles as carrier transport layers and electrodes. Most recently, UV PDs based on colloidal ZnO quantum dots and graphene nanocomposites were fabricated on poly(ethylene terephthalate) (PET) sheets (Figure 3c).<sup>[38]</sup> The UV PD under illumination at 365 nm wavelength and 3 V showed ratios of the photocurrent to dark current of approximately  $1.1 \times 10^4$ . The rise and the decay times of the UV PD were approximately 2 and 1 s, respectively (Figure 3d). Furthermore, nanoparticle-modified semiconductor films are a potential alternative for UV PDs. A solution-processed UV PD with a PVK:ZnO nanocomposite active layer composed of ZnO nanoparticles blended with semiconducting polymers can significantly outperform inorganic PDs (Figure 3e).<sup>[39]</sup> The PVK:ZnO nanocomposite film-based PD shows a very low dark current of 6.8 nA at an applied voltage of  $-9.0$  V, and a photocurrent of ca. 70 mA when the wavelength of the light source is 360 nm ( $1.25 \text{ mW cm}^{-2}$ ; Figure 3f). This kind of nanocomposite structure-based UV PD has great potential for replacing inorganic UV PDs and for opening avenues to new applications.

## 2.5. Self-Powered UV PDs

As a new field in self-powered nanotechnology-related research, self-powered UV PDs have been developed. They can be self-powered by harvesting energy from the environment and operate independently without using batteries, which can not only greatly enhance the adaptability of the devices but also greatly reduce the size and weight of the systems. Generally, these designed self-powered PDs include two classes. One type of self-powered PD is powered by an integrated energy harvesting unit, which is usually equipped

with a capacitor; for instance, Wang et al. developed a self-powered UV PD by integrating a micrometer-sized biofuel cell (BFC) and a nanogenerator (NG) with a ZnO NW-based sensor (Figure 4a-d).<sup>[58]</sup> The BFC and the NG concurrently harvest mechanical and biochemical energy, and then power the UV PD. When UV light is shining on the UV PD, its resistance decreases because of the increasing number of carriers, and the voltage drop on the PD decreases accordingly. By monitoring the voltage drop on the UV PD, UV light can be detected quantitatively (Figure 4e).

Another type of self-powered UV PD has been developed by exploiting the photovoltaic effect. The type of self-powered UV PD not only detects signals but also is powered by those signals; the devices exhibit a much faster photoresponse speed and a higher photosensitivity than the conventional photoconductive UV PDs and shows potential applications in light detecting and nano-optoelectronic integrated circuits. Cho et al. fabricated a self-powered UV photovoltaic device based on a single-crystalline nanowire ZnO  $p$ - $n$  homojunction.<sup>[59]</sup> At zero-voltage bias, the dark current was less than 1 pA and the open-circuit voltage ( $V_{OC}$ ) was 0 V, whereas the photocurrent was ca. 1  $\mu$ A and the  $V_{OC}$  was ca. 0.2 V under UV light illumination. The rise time during the voltage-increasing edge and the decay time were estimated to be 30 and 50 ms, respectively, which are smaller than those of the previously reported photoconductive ZnO UV PDs.<sup>[60]</sup> Liao et al. reported an ultrafast and visible-blind UV PD based on ZnO/GaN nanoscale  $p$ - $n$  junctions.<sup>[61]</sup> The self-powered visible-blind UV PD had an ultrafast response of rise time (ca. 20  $\mu$ s) and decay time (ca. 219  $\mu$ s), which is two orders of magnitude faster than ZnO photoconductivity-based PDs. The UV PD was driven by the photovoltaic effect of the ZnO/GaN  $p$ - $n$  junction with a UV photocurrent of ca.  $2 \times 10^{-6}$  A and a  $V_{OC}$  of  $\sim 2.7$  V at zero bias.

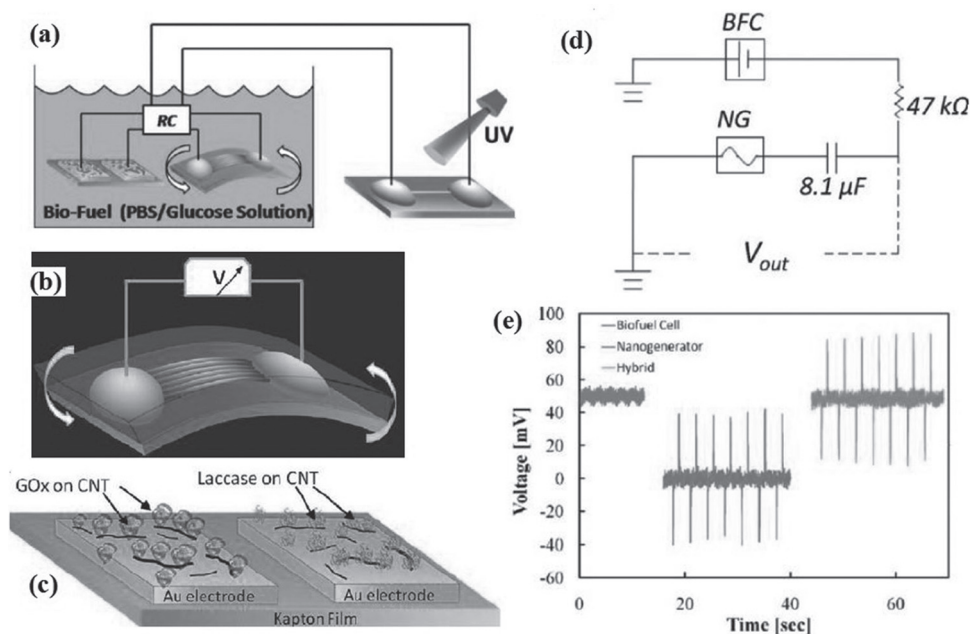


**Figure 4.** a) Schematic illustration of the self-powered UV PD. b) Mechanical bending of the NG creates tensile strain and a corresponding piezoelectric field along the fiber that drives the electrons through an external load back and forth following the cycled mechanical action. c) Schematic illustration of the fabricated BFC device. d) Circuit diagram used for integration of the hybrid BFC-NG device. Note, considering the inner resistance of the NG, the time required to charge the capacitor is much longer than the period at which the strain was applied to the NG, so that the output  $V$  is a sum of those from BFC and NG. e) Open-loop voltage of the independent and combined operation of the BFC and PVDF NG. Reproduced with permission.<sup>[58]</sup> Copyright 2010, ACS.

### 3. Conclusion and Outlook

In summary, the state-of-the-art research activities on LD nanostructure-based visible-blind UV PDs have been reviewed. LD nanostructure-based visible-blind UV PDs exhibit a much faster photoresponse speed and a higher photosensitivity, and show potential applications in light detecting and nano-optoelectronic integrated circuits. However, there still is a lot of room for the development of LD nanostructures and their PD application in this field. Therefore, considerable interest in the future study of fabricating LD nanostructure-based visible-blind UV PDs is proposed. First, the growth kinetics and thermodynamics involved in the synthesis of LD nanostructures are extremely complex, and significant challenges still exist in the synthesis of high-quality LD nanostructures, including reliable control of diameter, length, orientation, density, crystallization and hierarchical assembly; new fabricating technologies need to be developed for the controlled growth and assembly of low-dimensional nanostructures. Second, constructing LD nanostructure devices uses some sophisticated techniques, such as photolithography and electron beam lithography, which are complicated, time-consuming, and costly, and thus hamper the development of practical manufacturing routes; a simple and effective method to construct UV PDs is highly desirable. Third, and finally, next generation UV PDs will require significant improvements in sensitivity, selectivity, and stability in order to meet the future demands of a variety of fields. Though some research groups have successfully fabricated LD nanostructure-based visible-blind UV PDs, the selectivity and stability are still quite low. It is believed that future research work in this field

will further enhance the photoconductor properties up to the level desirable in practical industrial application.

### Acknowledgements

This work was supported by the National Basic Research Program of China (grant no. 2012CB932303), the Postdoctoral Science Foundation of China (2012M520825), the National Natural Science Foundation of China (91123006, 21001028, and 51002032), Shanghai Chenguang Foundation (11CG06), Shanghai Pujiang Program (11PJ1400300, 12PJ1400300), Shanghai Shu Guang Project (12SG01), the Science and Technology Commission of Shanghai Municipality (11520706200), the Programs for Professor of Special Appointment (Eastern Scholar) at Shanghai Institutions of Higher Learning, and the New Century Excellent Talents in University (NCET-11-0102).

Received: April 23, 2013  
Published online: June 21, 2013

- [1] X. S. Fang, Y. Bando, U. K. Gautam, T. Y. Zhai, H. B. Zeng, X. J. Xu, M. Y. Liao, D. Golberg, *Crit. Rev. Solid State Mater. Sci.* **2009**, *34*, 190.
- [2] Y. Taniyasu, M. Kasu, T. Makimoto, *Nature* **2006**, *441*, 325.
- [3] M. Razeghi, A. Rogalski, *J. Appl. Phys.* **1996**, *79*, 7433.
- [4] L. K. Wang, Z. G. Ju, J. Y. Zhang, J. Zheng, D. Z. Shen, B. Yao, D. X. Zhao, Z. Z. Zhang, B. H. Li, C. X. Shan, *Appl. Phys. Lett.* **2009**, *95*, 131113.
- [5] M. Law, D. J. Sirbully, J. C. Johnson, J. Goldberger, R. J. Saykally, P. D. Yang, *Science* **2004**, *305*, 1269.
- [6] L. Li, P. C. Wu, X. S. Fang, T. Y. Zhai, L. Dai, M. Y. Liao, Y. Koide, H. Q. Wang, Y. Bando, D. Golberg, *Adv. Mater.* **2010**, *22*, 3161.

- [7] X. S. Fang, Y. Bando, M. Y. Liao, U. K. Gautam, C. Y. Zhi, B. Dierre, B. D. Liu, T. Y. Zhai, T. Sekiguchi, Y. Koide, D. Golberg, *Adv. Mater.* **2009**, *21*, 2034.
- [8] X. S. Fang, S. L. Xiong, T. Y. Zhai, Y. Bando, M. Y. Liao, U. K. Gautam, Y. Koide, X. G. Zhang, Y. T. Qian, D. Golberg, *Adv. Mater.* **2009**, *21*, 5016.
- [9] S. Liu, J. F. Ye, Y. Cao, Q. Shen, Z. F. Liu, L. M. Qi, X. F. Guo, *Small* **2009**, *4*, 2371.
- [10] C. S. Lao, M. C. Park, Q. Kuang, Y. L. Deng, A. K. Sood, D. L. Polla, Z. L. Wang, *J. Am. Chem. Soc.* **2007**, *129*, 12096.
- [11] C. Soci, A. Zhang, B. Xiang, S. A. Dayeh, D. P. R. Aplin, J. Park, X. Y. Bao, Y. H. Lo, D. Wang, *Nano Lett.* **2007**, *7*, 1003.
- [12] H. Kind, H. Q. Yan, B. Messer, M. Law, P. D. Yang, *Adv. Mater.* **2002**, *14*, 158.
- [13] S. E. Ahn, H. J. Ji, K. Kim, G. T. Kim, C. H. Bae, S. M. Park, Y. K. Kim, J. S. Ha, *Appl. Phys. Lett.* **2007**, *90*, 153106.
- [14] J. P. Cheng, Y. J. Zhang, R. Y. Guo, *J. Cryst. Growth* **2008**, *310*, 57.
- [15] J. Zhou, Y. D. Gu, Y. F. Hu, W. J. Mai, P. H. Yeh, G. Bao, A. K. Sood, D. L. Polla, Z. L. Wang, *Appl. Phys. Lett.* **2009**, *94*, 191103.
- [16] J. B. K. Law, J. T. L. Thong, *Appl. Phys. Lett.* **2006**, *88*, 133114.
- [17] S. E. Ahn, J. S. Lee, H. Kim, S. Kim, B. H. Kang, K. H. Kim, G. T. Kim, *Appl. Phys. Lett.* **2004**, *84*, 5022.
- [18] J. Y. Park, Y. S. Yun, Y. S. Hong, H. Oh, J. J. Kim, S. S. Kim, *Appl. Phys. Lett.* **2005**, *87*, 123108.
- [19] C. C. Lin, W. H. Lin, Y. Y. Li, *J. Nanosci. Nanotechnol.* **2009**, *9*, 2813.
- [20] Y. J. Chen, C. L. Zhu, M. S. Cao, T. H. Wang, *Nanotechnology* **2007**, *18*, 285502.
- [21] C. H. Lin, R. S. Chen, T. T. Chen, H. Y. Chen, Y. F. Chen, K. H. Chen, L. C. Chen, *Appl. Phys. Lett.* **2008**, *93*, 112115.
- [22] J. M. Wu, C. H. Kuo, *Thin Solid Films* **2009**, *517*, 3870.
- [23] Q. Kuang, C. S. Lao, Z. Li, Y. Z. Liu, Z. X. Xie, L. S. Zheng, Z. L. Wang, *J. Phys. Chem. C* **2008**, *112*, 11539.
- [24] P. Feng, J. Y. Zhang, Q. H. Li, T. H. Wang, *Appl. Phys. Lett.* **2006**, *88*, 153107.
- [25] D. Zhang, C. Li, S. Han, X. Liu, T. Tang, W. Jin, C. Zhou, *Appl. Phys. A* **2003**, *77*, 163.
- [26] X. Q. Fu, C. Wang, P. Feng, T. H. Wang, *Appl. Phys. Lett.* **2007**, *91*, 073104.
- [27] X. Y. Xue, T. L. Guo, Z. X. Lin, T. H. Wang, *Mater. Lett.* **2008**, *62*, 1356.
- [28] P. Feng, J. Y. Zhang, Q. Wan, T. H. Wang, *J. Appl. Phys.* **2007**, *102*, 074309.
- [29] C. C. Lin, Y. W. Chen, M. C. Chiang, C. H. Lee, Y. L. Tung, S. Y. Chen, *J. Electrochem. Soc.* **2010**, *157*, H227.
- [30] X. S. Fang, L. F. Hu, K. F. Huo, B. Gao, L. J. Zhao, M. Y. Liao, P. K. Chu, Y. Bando, D. Golberg, *Adv. Funct. Mater.* **2011**, *21*, 3907.
- [31] L. F. Hu, J. Yan, M. Y. Liao, H. J. Xiang, X. G. Gong, L. D. Zhang, X. S. Fang, *Adv. Mater.* **2012**, *24*, 2305.
- [32] L. F. Hu, J. Yan, M. Y. Liao, L. Wu, X. S. Fang, *Small* **2011**, *7*, 1012.
- [33] L. F. Hu, M. Chen, W. Z. Shan, T. R. Zhan, M. Y. Liao, X. S. Fang, X. H. Hu, L. Wu, *Adv. Mater.* **2012**, *24*, 5872.
- [34] M. Chen, L. F. Hu, J. X. Xu, M. Y. Liao, L. Wu, X. S. Fang, *Small* **2011**, *7*, 2449.
- [35] X. S. Fang, Y. Bando, M. Y. Liao, T. Y. Zhai, U. K. Gautam, L. Li, Y. Koide, D. Golberg, *Adv. Funct. Mater.* **2010**, *20*, 500.
- [36] L. Li, P. S. Lee, C. Y. Yan, T. Y. Zhai, X. S. Fang, M. Y. Liao, Y. Koide, Y. Bando, D. Golberg, *Adv. Mater.* **2010**, *22*, 5145.
- [37] Y. Z. Jin, J. P. Wang, B. Q. Sun, J. C. Blakesley, N. C. Greenham, *Nano Lett.* **2008**, *8*, 1649.
- [38] D. I. Son, H. Y. Yang, T. W. Kim, W. Park, *Appl. Phys. Lett.* **2013**, *102*, 021105.
- [39] F. Guo, B. Yang, Y. B. Yuan, Z. G. Xiao, Q. F. Dong, Y. Bi, J. S. Huang, *Nature Nanotech.* **2012**, *7*, 798.
- [40] M. Y. Liao, Y. Koide, *Appl. Phys. Lett.* **2006**, *89*, 113509.
- [41] R. Suzuki, S. Nakagomi, Y. Kokubun, *Appl. Phys. Lett.* **2011**, *98*, 131114.
- [42] S. Han, Z. Zhang, J. Y. Zhang, L. K. Wang, J. Zheng, H. F. Zhao, Y. Zhang, M. M. Jiang, S. P. Wang, D. X. Zhao, C. X. Shan, B. H. Li, D. Z. Shen, *Appl. Phys. Lett.* **2011**, *99*, 242105.
- [43] Z. G. Ju, C. X. Shan, D. Y. Jiang, J. Y. Zhang, B. Yao, D. X. Zhao, D. Z. Shen, X. W. Fan, *Appl. Phys. Lett.* **2008**, *93*, 173505.
- [44] Y. N. Hou, Z. X. Mei, Z. L. Liu, T. C. Zhang, X. L. Du, *Appl. Phys. Lett.* **2011**, *98*, 103506.
- [45] E. Monroy, F. Calle, J. A. Garrido, P. Youinou, E. Munoz, F. Omn'es, B. Beaumont, P. Gibart, *Semicond. Sci. Technol.* **1999**, *14*, 685.
- [46] X. S. Fang, L. Wu, L. F. Hu, *Adv. Mater.* **2011**, *23*, 585.
- [47] L. F. Hu, M. Chen, X. S. Fang, L. Wu, *Chem. Soc. Rev.* **2012**, *41*, 1350.
- [48] X. S. Fang, Y. Bando, U. K. Gautam, C. H. Ye, D. Golberg, *J. Mater. Chem.* **2008**, *18*, 509.
- [49] T. Y. Zhai, X. S. Fang, M. Y. Liao, X. J. Xu, H. B. Zeng, Y. Bando, D. Golberg, *Sensors* **2009**, *9*, 6504.
- [50] P. D. Yang, R. X. Yan, M. Fardy, *Nano Lett.* **2010**, *10*, 1529.
- [51] S. Liang, H. Sheng, Y. Liu, Z. Huo, Y. Lu, H. Shen, *J. Cryst. Growth* **2001**, *225*, 110.
- [52] T. Tut, T. Yelboga, E. Ulker, E. Ozbay, *Appl. Phys. Lett.* **2008**, *92*, 103502.
- [53] I. K. Sou, M. C. W. Wu, T. Sun, K. S. Wong, G. K. L. Wong, *Appl. Phys. Lett.* **2001**, *78*, 1811.
- [54] J. Xing, E. Guo, K. J. Jin, H. B. Lu, J. Wen, G. Z. Yang, *Opt. Lett.* **2009**, *34*, 1675.
- [55] M. R. Werner, W. R. Fahmer, *IEEE Trans. Ind. Electron.* **2001**, *48*, 249.
- [56] P. Sharma, K. Sreenivas, K. V. Rao, *J. Appl. Phys.* **2003**, *93*, 3963.
- [57] R. Ghosh, B. Mallik, D. Basak, *Appl. Phys. A* **2005**, *81*, 1281.
- [58] B. J. Hansen, Y. Liu, R. Yang, Z. L. Wang, *ACS Nano* **2010**, *4*, 3647.
- [59] H. Cho, A. S. Zakirov, S. U. Yuldashev, C. W. Ahn, Y. K. Yeo, T. W. Kang, *Nanotechnology* **2012**, *23*, 115401.
- [60] O. Lupan, G. Chai, L. Chow, G. A. Emelchenko, H. Heinrich, V. V. Ursaki, A. N. Gruzintsev, I. M. Tiginyanu, A. N. Redkin, *Phys. Status Solidi A* **2010**, *207*, 1735.
- [61] Y. Q. Bie, Z. M. Liao, H. Z. Zhang, G. R. Li, Y. Ye, Y. B. Zhou, J. Xu, Z. X. Qin, L. Dai, D. P. Yu, *Adv. Mater.* **2011**, *23*, 649.